scientific reports

Check for updates

OPEN

Field direction of static magnetic fields influences kidney fibrosis progression through MAPK signaling and cell cycle alteration

Seong Min Lee[1,15], Saram Lee[2,3,4,15], Kyu Hyeon Kim[1], Daehan Kim[5], Seong Joon Park[1], Kyu Hong Kim[1], Sunhwa Lee[6], Eunjin Bae[7], Kyung Don Yoo[8], Jae Wook Lee[9], Joong Yull Park[5], Yon Su Kim[10,11,12], Ran-hui Cha[13,14]✉ & Seung Hee Yang[12,13]✉

Various mechanisms, including inflammation, oxidative stress, and apoptosis, are involved in the transition from acute kidney injury to chronic kidney disease (AKI-to-CKD). In this study, we aimed to determine the pathway linking acute injury and fibrosis under static magnetic fields (SMFs). Human tubular epithelial cells (hTECs) were cultured on SMF platforms (119 mT; outward vs. inward direction) for 3 days, followed by treatment with adenine and p38 mitogen-activated protein kinase (MAPK) inhibitor to verify the role of MAPK pathway. In-vivo, mice were orally administered adenine (2mg/mouse/day) for 14 days to induce tubular injury, and p38 MAPK inhibitor (iP38, 10mg/kg) was injected intraperitoneally to evaluate its therapeutic effect. Inward SMF exposure significantly increased phospho-p38 (pp38) expression compared to outward SMFs. p38 MAPK inhibition reduced G1/S arrest and oxidative stress, apoptosis, and expression of fibrosis markers under inward SMFs. Additionally, iP38 treatment alleviated inflammation and fibrosis in adenine-induced tubular nephropathy (AITN). This study revealed that SMF-related AKI-to-CKD transition progresses with the direction of SMFs affecting the severity of injury, whereas p38 MAPK inhibition attenuates SMF-induced kidney injury and prevents fibrosis.

Keywords AKI-to-CKD, Cell cycle, Mitogen-activated protein pathway, Static magnetic field

The increasing utilization of magnetic resonance imaging (MRI) for diagnosing diseases has raised significant concerns regarding the potential effects of magnetic fields on human health. MRI machines typically used in hospitals have magnetic field strengths ranging from 3 to 9.4 Tesla[1]. Recently, to achieve higher resolutions, MRI machines with even stronger magnetic field strengths have been developed. Milovanovich et al. reported that an upward-oriented static magnetic field (SMF) induced brain edema and increased spleen cellularity, whereas the downward-oritented SMF led to liver inflammation and a reduction in serum granulocyte levels[2]. However, in a cisplatin-induced nephrotoxicity model, moderate SMFs at hundreds of mT attenuated kidney injury by reducing oxidative stress and inflammation[3]. The effects of SMFs can be variable according to their

[1]Department of Biomedical Sciences, Seoul National University, Seoul, Republic of Korea. [2]Department of Transdisciplinary Medicine, Seoul National University Hospital, Seoul, Republic of Korea. [3]Department of Medicine, Seoul National University College of Medicine, Seoul, Republic of Korea. [4]Innovative Medical Technology Research Institute, Seoul National University Hospital, Seoul, Republic of Korea. [5]Department of Medical Engineering, Graduate School, Chung-Ang University, Seoul, Republic of Korea. [6]Division of Nephrology, Department of Internal Medicine, Kangwon National University Hospital, Chuncheon, Republic of Korea. [7]Institute of Medical Science, College of Medicine, Gyeongsang National University, Jinju, Republic of Korea. [8]Department of Internal Medicine, Ulsan University Hospital, University of Ulsan College of Medicine, Ulsan, Republic of Korea. [9]Nephrology Clinic, National Cancer Center of Korea, Goyang, Republic of Korea. [10]Department of Internal Medicine, Seoul National University Hospital, Seoul, Republic of Korea. [11]Department of Internal Medicine, Seoul National University College of Medicine, Seoul, Republic of Korea. [12]Department of Kidney Research Institute, Seoul National University Medical Research Center, Seoul, Republic of Korea. [13]Biomedical Research Institute, Seoul National University Hospital, 101, Daehak-ro, Jongno-gu, Seoul, Republic of Korea. [14] Division of Nephrology, Department of Internal Medicine, National Medical Center, Seoul, Republic of Korea. [15]Seong Min Lee and Saram Lee have contributed equally to this study as first authors. ✉email: reginaprayer@gmail.com; ysh5794@snu.ac.kr

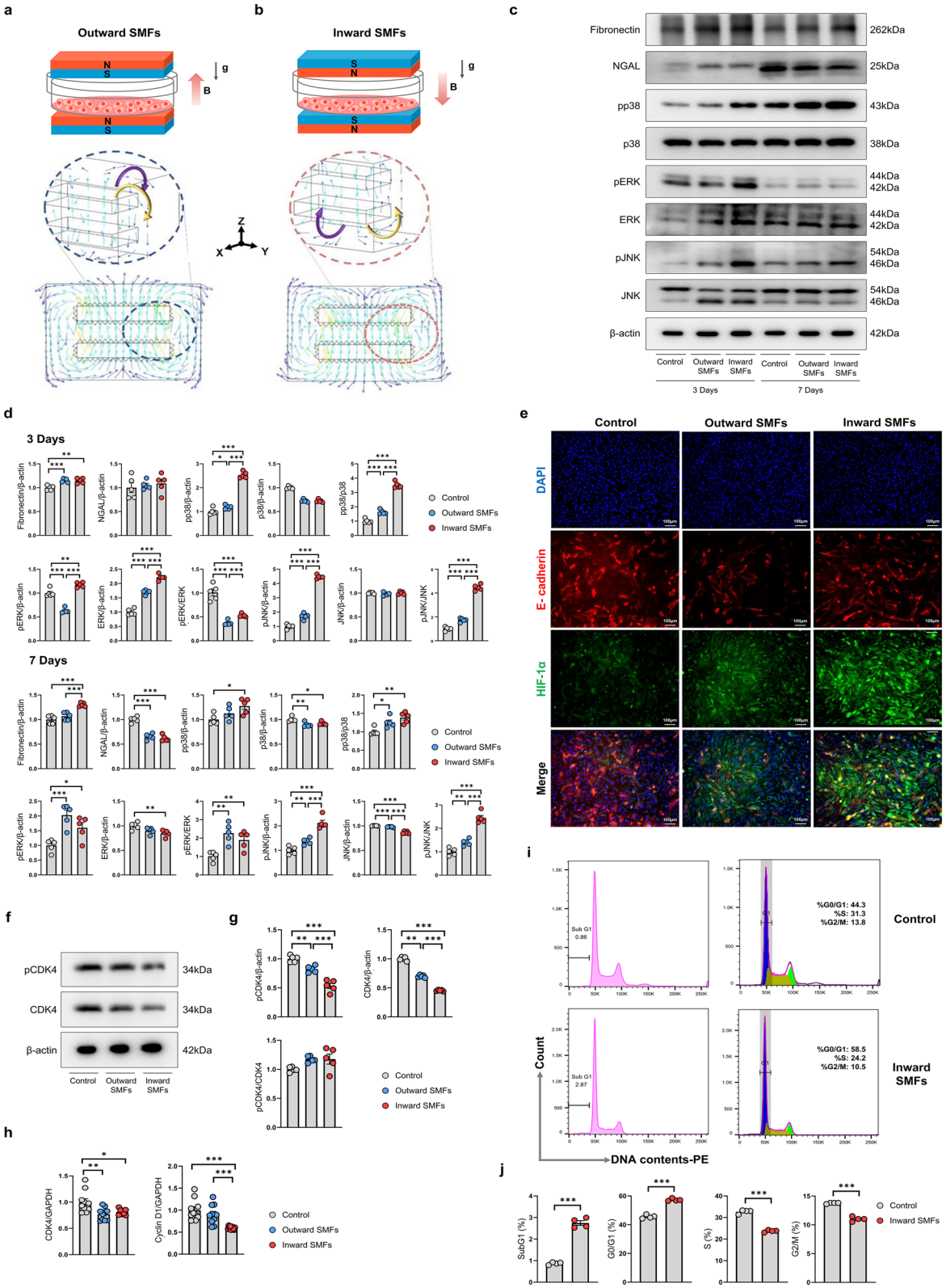

particular characteristics, including shape, strength, direction, and cell type. The exact mechanisms also remain inconclusive owing to the complicated effects of magnetic fields on biological systems.

Acute kidney injury (AKI) affects 5–10% of hospitalized patients, leading to kidney tissue damage, elevated blood creatinine levels, and reduced urine output[4,5]. Over the past decade, increasing evidence has indicated that AKI is a significant contributor to the development of chronic kidney disease (CKD)[6]. The AKI-to-CKD transition involves complex mechanisms primarily driven by maladaptive repair processes, including cell cycle arrest, inflammation, and fibrosis[6].

◀**Fig. 1**. Inward SMF exposure induced tubular epithelial injury by modulating the MAPK pathway and triggering G1/S phase arrest. **a**, **b** Schematic design of experiments and magnetic field distribution. hTECs were exposed to outward SMFs (**a**) or inward SMFs (**b**) for 3 or 7 days. **c**, **d** Western blot representative images (**c**) and quantification (**d**) of fibronectin, NGAL, pp38, p38, pERK, ERK, pJNK, and JNK. **e** Reduced expression of E-cadherin and elevated expression of HIF-1α were observed via immunofluorescence staining under exposure to SMFs for 3 days, particularly in the inward direction. Scale bars, 100 μm (×100). **f**, **g** Western blot results of pCDK4 and CDK4 expression in hTECs. **h** Relative mRNA expression levels of CDK4 and cyclin D1 (n = 10 in each group). **i** Flow cytometry showing alterations in cell cycle distribution following exposure to inward SMFs. **j** Quantification of the percentage of cells in each phase of the cell cycle. The experiments were independently replicated at least three times, with the data presented as mean ± SEM. $^{*}P < 0.05$, $^{**}P < 0.01$, $^{***}P < 0.001$.

The p38 mitogen-activated protein kinase (MAPK), a serine/threonine protein kinase, is involved in crucial intracellular signal transduction pathways and plays a significant role in the pathogenesis of fibrosis[7]. In response to cellular stress, p38 MAPK can translocate to the nucleus and subsequently induce the activation of transcription factors contributing to the production of proinflammatory mediators[8]. Previous studies have demonstrated that inhibiting p38 MAPK may protect kidneys from injury and attenuate disease progression in various models[8–10]. Furthermore, p38 MAPK activation was reportedly associated with kidney interstitial fibrosis in a unilateral ureteral obstruction (UUO) mouse model, and the anti-fibrotic effect of p38 MAPK inhibition has been confirmed[10].

To our knowledge, there have been no reports regarding the differential effect of SMF directions on kidney tissues and the proper damage mechanisms. In this study, we established an SMF-associated AKI model and observed the effects of magnetic field directions. Furthermore, we evaluated the role of p38 MAPK in AKI-to-CKD progression in a mouse model.

Results

SMFs induce tubular epithelial cell injury, especially under the inward direction

Simulations were conducted under two conditions by changing the polarity of the magnets: outward, where cells receive magnetic force from bottom up, and inward, where cells receive magnetic force from top down. In the outward condition, the maximum value of magnetic flux density was approximately 121.4 mT in the x–y plane 1 mm above the magnet (the plane where the cells were located). Within the range of the magnet, the maximum magnetic flux density of approximately 121.4 mT was observed at the tip of the magnet, whereas the minimum magnetic flux density of approximately 105.6 mT was observed at the center of the magnet (the difference of 13.0%). Thesimulation results for the inward condition were identical to those for the outward condition, with the sole difference being the reversal of the direction of the magnetic flux density vector. Vertically upward and downward SMFs formed an outward and inward direction of SMFs, respectively (Fig. 1a, b). To verify the reliability of the magnetic field simulation results, the simulated magnetic flux density values at each location were compared with the actual magnetic field measurements. The magnetic field strengths measured at 15, 30, and 45 mm along the y-axis of the magnet were approximately 114.8, 110, and 112.1 mT, respectively, and the simulation results at those points were 112.0, 106.1, and 112.1 mT, respectively, with an average error of approximately 2.0% between the measured and simulated results, indicating that the simulation results were considered reliable.

Using a magnetic field analyzer, the intensity of the SMFs was measured to be approximately 119 mT under both orientations. We initially investigated the effects of SMFs at both early and late stages by culturing with SMFs for either 3 or 7 days. By the 7th day, the vast majority of cells were dead. After 3 days of exposure, we noticed an elevation in fibrosis marker fibronectin, the kidney injury marker neutrophil gelatinase-associated lipocalin (NGAL), as well as elevated protein levels of phospho-p38 (pp38), phospho-extracellular-signal-regulated kinase (pERK), and phospho-c-Jun N-terminal kinase (pJNK), with these effects being more pronounced under inward SMFs than outward SMFs. These findings suggest that inward SMFs may promote fibrosis by modulating the p38 MAPK signaling pathway (Fig. 1c, d). Immunofluorescence assay revealed that exposure to both outward and inward SMFs for 3 days led to decreased expression of intercellular junction marker E-cadherin and increased levels of hypoxia-inducible factor-1α (HIF-1α), with more pronounced alterations under inward SMFs. This suggests that SMFs induced AKI-to-CKD transition by regulating inflammation and oxidative stress through HIF-1α signaling. HIF-1α elevation implies oxygen deprivation in cells exposed to SMFs (Fig. 1e). Moreover, protein levels of both phospho-cyclin-dependent kinase-4(pCDK4) and CDK4, the key regulators of the G1/S phase transition in the cell cycle, were significantly reduced under both SMF conditions compared to the control. Notably, inward SMFs led to a stronger reduction compared to outward SMFs (Fig. 1f, g). Similarly, CDK4 mRNA levels were decreased under both inward and outward SMFs relative to the control, with no significant difference observed between the two conditions. However, cyclin D1 mRNA levels were uniquely reduced under inward SMFs than under outward SMFs (Fig. 1h).

To further investigate whether the downregulation of cell cycle regulators leads to cell cycle arrest, we performed flow cytometric analysis using propidium iodide (PI) staining. The proportion of cells in the G0/G1 phase significantly increased under inward SMFs from 45.55 ± 0.63 to 57.23 ± 0.44 ($^{***}P < 0.001$) (Fig. 1f, g). In line with the significant increase in pp38 expression and the proportion of cells in the G0/G1 phase under inward SMFs, these findings imply that exposure to inward SMFs induced tubular epithelial injury by modulating the p38 MAPK pathway and inducing G1/S phase arrest. In particular, the directionality of SMFs appears to play a critical role in mediating these cellular responses.

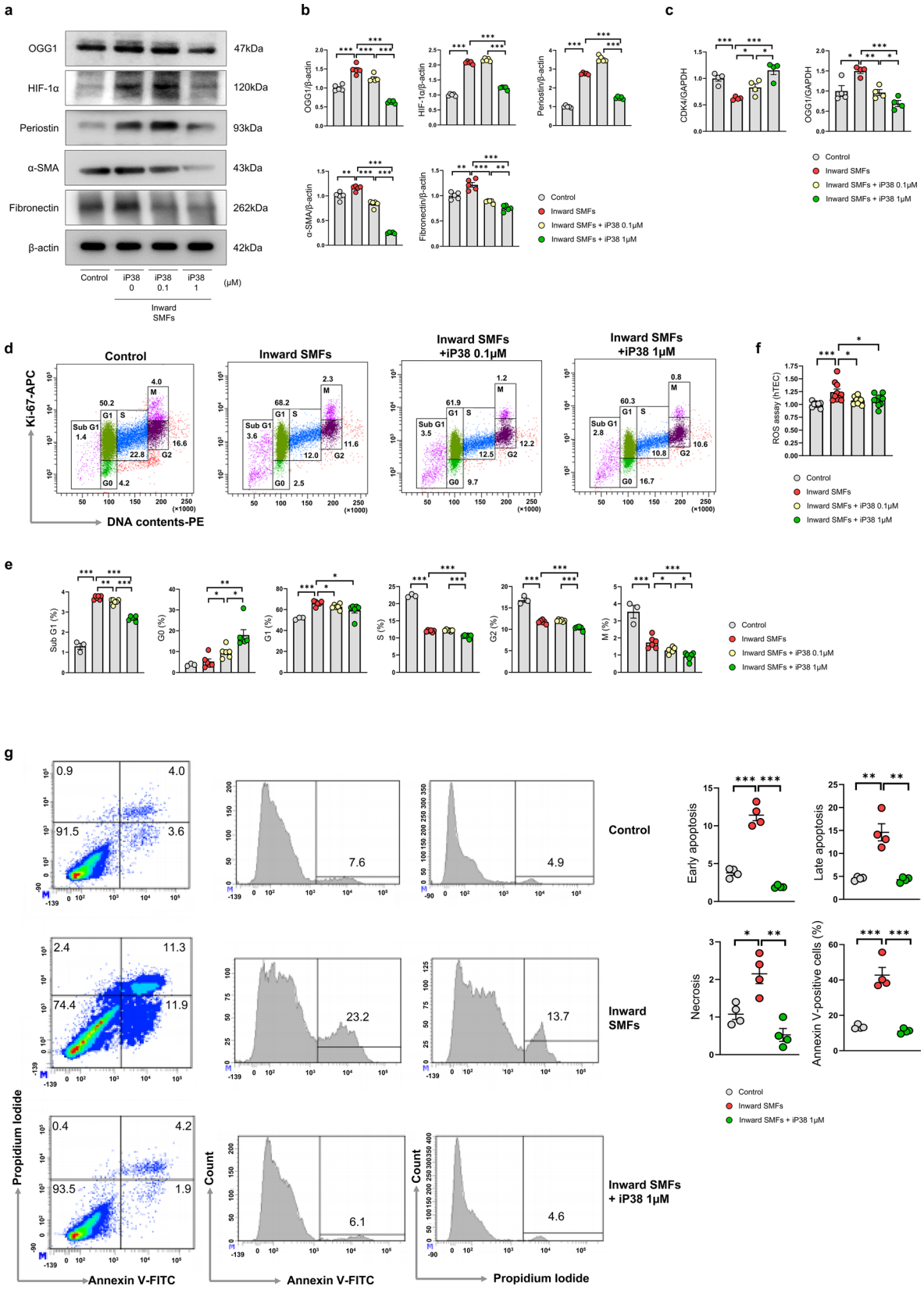

p38 MAPK inhibitor protected against tubular damage induced by inward SMFs

To examine the therapeutic potential of p38 MAPK inhibition in tubular epithelial cells exposed to inward SMFs, we treated human primary tubular epithelial cells (hTECs) with iP38 (0.1 μM, 1 μM) while concomitantly exposing them to inward SMFs for 3 days. p38 MAPK inhibitor treatment considerably reduced the expression of 8-oxoguanine DNA glycosylase 1 (OGG1), a marker of DNA damage and oxidative stress, compared with inward SMFs alone. Additionally, HIF-1α and fibrosis markers including periostin, α-smooth muscle actin

◀**Fig. 2**. Inhibition of p38 protected tubular epithelial cells from inward SMF-induced tubular damage. **a**, **b** Western blot representative images (**a**) and quantification (**b**) for OGG1, HIF-1α periostin, α-SMA, and fibronectin. **c** mRNA levels of CDK4 and OGG1 were analyzed using real-time qPCR (n = 4 in each group). **d** Representative images of cell cycle analysis by PI and Ki-67 staining (n = 3–6 in each group). **e** Proportions of HK-2 cells in each phase of the cell cycle quantified as percentages. **f** Intracellular ROS levels were assessed under inward SMFs and iP38 treatment. **g** Increased ratios of apoptotic cells were observed with inward SMF exposure, which decreased following treatment with a p38 MAPK inhibitor. Early apoptosis, late apoptosis, necrosis, and combined cell proportions were assessed under inward SMF exposure and p38 MAPK inhibition. The experiments were independently replicated at least three times, and the data are presented as mean ± SEM. Statistical significance is indicated as $^{*}P < 0.05$, $^{**}P < 0.01$, $^{***}P < 0.001$.

(α-SMA), and fibronectin markedly increased with inward SMF exposure but iP38 treatment attenuated this increase (Fig. 2a, b). The mRNA expression of CDK4 was downregulated by inward SMFs but was recovered following iP38 treatment. The increased OGG1 mRNA expression under inward SMFs also decreased after iP38 treatment (Fig. 2c). This indicates that p38 MAPK inhibition prevented cell cycle arrest in the G1/S phase induced by inward SMFs. The proportion of cells in the G1 phase significantly increased under inward SMFs compared with those in the control group (51.57 ± 0.68 vs 66.05 ± 0.97, $^{***}P < 0.001$; control vs inward SMFs). However, the increase was reduced with iP38 treatment of 0.1 μM and 1 μM, respectively (66.05 ± 0.97 vs 62.7 ± 1.02, $^{*}P < 0.05$, 59.35 ± 2.64, $^{*}P < 0.05$; inward SMFs vs inward SMFs + iP38 0.1 μM, inward SMFs + iP38 1 μM). Additionally, the proportion of cells in the sub G1 phase increased by 2.85-fold following inward SMF exposure compared with those in the control group, indicating an increase in apoptotic cells (1.3 ± 0.15 vs 3.72 ± 0.04, $^{***}P < 0.001$; control vs inward SMFs). iP38 treatment significantly decreased the proportion of cells in the sub G1 phase in a dose-dependent manner (3.72 ± 0.04 vs 3.52 ± 0.05, $^{**}P < 0.01$, 2.68 ± 0.05, $^{***}P < 0.001$; inward SMFs vs inward SMFs + iP38 0.1 μM, inward SMFs + iP38 1 μM) (Fig. 2d, e). Consistent with these findings, p38 MAPK inhibition also suppressed the elevated intracellular reactive oxygen species (ROS) levels induced by inward SMFs (Fig. 2f). Furthermore, iP38 treatment mitigated the rise in apoptotic cells caused by inward SMFs, with a particularly notable reduction in early apoptotic cells (Fig. 2g). Overall, these results suggest that inhibiting p38 MAPK may reduce the tubular epithelial injury influenced by oxidative stress and G1/S arrest induced by inward SMFs.

Inhibition of p38 MAPK mitigated fibrosis in adenine-induced tubular nephropathy (AITN) model

To mimic CKD progression, we established an AITN model by orally administering adenine to mice daily for two weeks (Fig. S1a). Adenine treatment resulted in elevated blood urea nitrogen (BUN) and serum creatinine levels (Fig. S1b), along with tubular injury and interstitial fibrosis (Fig. S1c, d). These changes were accompanied by increased expression of NGAL, F4/80^{+} macrophages infiltration, pp38, HIF-1α and pro-inflammatory and apoptotic markers, indicating AKI-to-CKD transition (Fig. S1c-e). To investigate the effects of p38 MAPK inhibition in the AITN model, mice received intraperitoneal injection of iP38 (a p38 MAPK inhibitor) 1 h prior to adenine administration (Fig. 3a). Body weight measurements revealed that adenine caused significant weight loss, while treatment of both iP38_S and iP38_D with adenine resulted in a slight increase in body weight (Fig. 3b). Gross morphology of adenine-treated kidneys showed irregular surfaces and coloration changes, indicative of extensive kidney injury, while iP38 treatment preserved kidney morphology, restoring both shape and color (Fig. 3c). Likewise, iP38 treatment significantly reduced blood urea nitrogen (BUN) and serum creatinine levels to 86.02 ± 9.60 mg/dL ($^{*}P < 0.05$) and 0.66 ± 0.08 mg/dL ($^{*}P < 0.05$), respectively (Fig. 3d). Histological images of adenine-treated kidneys revealed enlarged basement membranes, damaged brush borders, increased tubular atrophy, and aggravated interstitial fibrosis, which were alleviated upon p38 MAPK inhibition. NGAL expression and F4/80^{+} macrophage infiltration was also reduced by suppressing p38 MAPK (Fig. 3e, f). In western blots, inhibiting p38 MAPK reduced the expression ratio of pp38 to p38, which was accompanied by reduced levels of fibronectin, the key extracellular matrix during kidney fibrosis, along with modulated p53 and NGAL expression. Interestingly, suppressing p38 MAPK also led to the decrease in pERK and pJNK protein levels (Fig. 3g).

To further investigate the role of p38 MAPK inhibition in an in-vitro AITN model, we treated hTECs with adenine and a p38 MAPK inhibitor. iP38 treatment significantly decreased the expression of fibronectin, periostin, and intercellular adhesion molecule-1 (ICAM-1), which are associated with fibrosis and inflammation (Fig. 3i, j). Moreover, we applied the same treatment under inward SMF conditions to assess the contribution of p38 MAPK to SMFs-related fibrotic response. While inward SMFs markedly increased the expression of fibronectin, periostin, and ICAM-1, co-treatment with iP38 significantly attenuated these increases induced by inward SMFs and adenine (Fig. 3k, l). These findings support a central role for p38 MAPK in mediating both adenine- and SMF-induced fibrotic responses in the kidney.

Discussion

In this study, we aimed to identify the pathway linking acute renal tubule injury caused by SMF exposure to fibrosis. First, we found that exposure to SMFs triggers tubular epithelial injury, which leads to fibrosis by altering the p38 MAPK pathway and inducing G1/S phase arrest. In addition, the direction of SMFs plays a significant role in these effects. Second, we confirmed the involvement of the p38 MAPK pathway by demonstrating the protective effect of its inhibition against SMF-induced tubular damage, as evidenced by reduced cell cycle arrest, oxidative stress, apoptosis, and decreased expression of fibrosis markers. Third, in a mouse AITN model, we

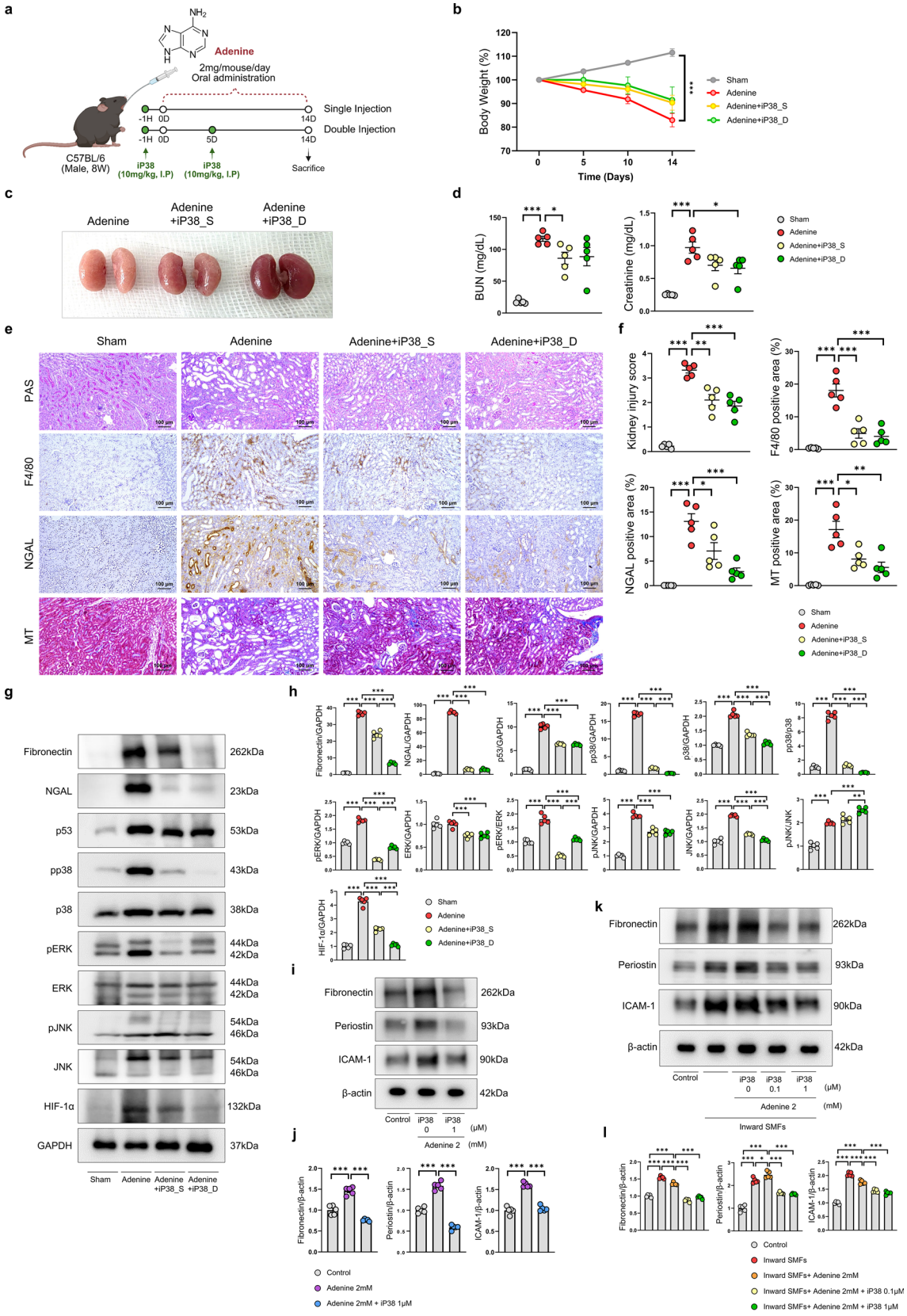

observed elevated levels of pp38 and kidney injury markers, which were markedly reduced by inhibition of p38 MAPK in the mouse AITN model. Furthermore, we observed a remarkable reduction in fibrosis markers through p38 MAPK inhibition in the in-vitro AITN model under inward SMFs. Overall, the study highlights the detrimental effects of SMF exposure on tubular epithelial cells, implicating the p38 MAPK pathway and cell cycle arrest in renal fibrosis, and suggests that the direction of magnetic fields plays an important role in the overall changes.

◀**Fig. 3**. p38 MAPK inhibitor attenuated fibrosis in AITN. **a** Schematic diagram illustrating p38 MAPK inhibition in the AITN model. **b** Body weight measurements during the experimental period (n = 5 in each group). **c** The gross morphology of kidneys was compared between the adenine-only, adenine + iP38_S, and adenine + iP38_D groups. **e**, **f** Representative IHC images (**e**) and quantitative analysis (**f**) of kidney sections including PAS, F4/80, NGAL, and MT staining (n = 5 in each group). Scale bars, 100 μm (× 100). **g**, **h** Western blot analysis showing that p38 MAPK inhibition reduced the expression of fibronectin, NGAL, p53, pp38, pERK, pJNK, and HIF-1α in kidney tissue. **i**, **j** Western blot results of hTECs treated with adenine and iP38. **k**, **l** Western blot analysis of fibrosis- and inflammation-related markers in hTECs cultured under inward SMFs and treated with adenine and iP38. The experiments were independently replicated at least three times, with the data presented as mean ± SEM. $^{*}P < 0.05$, $^{**}P < 0.01$, $^{***}P < 0.001$.

Kidney fibrosis is widely recognized as a common pathological consequence of CKD. When kidneys are injured, local pericytes and fibroblasts activate, secreting inflammatory mediators and synthesizing extracellular matrix components such as collagens and fibronectin[11]. Fibrosis develops with persistent accumulation of extracellular matrix proteins in cases of severe damage, accelerating the advancement of CKD through transforming growth factor-β (TGF-β) signaling[12]. Tissue hypoxia is common in CKD, and hypoxic signaling primarily involves HIFs, whose stability is increased under low-oxygen conditions owing to reduced prolyl hydroxylase-mediated degradation[13]. HIF-1α, a transcription factor, promotes collagen accumulation and facilitates the epithelial-to-mesenchymal transition[14,15]. Overexpression of HIF-1α in tubular epithelial cells promotes interstitial fibrosis in 5/6 nephrectomy mice[16], whereas silencing gene expression of HIF-1α reduced TGF-β induced epithelial-to-mesenchymal transition and angiotensin II-induced profibrotic effects in kidney cells[17]. Our experiment resulted in the upregulated expression of fibrosis markers and HIF-1α as well as the decreased expression of E-cadherin under inward SMFs, which is consistent with previous studies. HIF-1α contributes to inflammation, kidney damage, and fibrosis, which results in AKI-to-CKD transition[18]. Reduced levels of E-cadherin are also associated with renal fibrosis and CKD progression[19,20].

To model tubule injury and fibrosis, we utilized the SMF platform. SMFs can influence various cellular processes, including cell proliferation, cell viability, and cell cycle[21,22]. Previous studies have reported that the cellular effects induced by SMFs vary according to the intensity and the direction of magnetic fields as well as cell types[23,24]. Tian et al. discovered that upward SMFs of 0.2–1T could effectively decrease the cell numbers of human tumor cell lines MCF7 and GIST-T1, whereas downward SMFs did not produce a notable impact. Interestingly, the leukemia cell numbers were reduced by both upward and downward SMFs. This study also revealed that the effects of SMFs were dependent on the direction of SMFs[24]. However, the intensity in both vertically upward and downward SMFs was not different at all, which was beyond expectations. In our experiments, vertically upward orientation resulted in the outward direction of SMFs, whereas vertically downward orientation resulted in the inward direction of SMFs. Inward SMFs markedly upregulated the expression of fibrosis marker and NGAL, and pp38, highlighting their strong profibrotic and proinflammatory effects. Given that the MAPK signaling pathway consists of three major branches, we further examined the expression of both total and phosphorylated forms of p38, ERK, and JNK[25–27]. Notably, after 3 days of inward SMFs exposure, significant increases were observed in pERK, ERK, and pJNK levels, which may indicate that inward SMFs broadly activate the MAPK cascade. These findings imply a possible link between inward SMFs and MAPK pathway activation, potentially contributing to fibrosis. Therefore, further studies using various orientations of SMFs and exposure conditions are needed to better understand the exact directional effects of SMFs on renal tubular cells.

The precise mechanisms underlying the different effects of SMF directions are still unclear[3,28]. Yu et al. showed that although both upward and downward SMFs reduce oxidative stress in the kidney, downward SMFs offer stronger protective effects by reducing kidney inflammation, apoptosis, and cisplatin accumulation via decreased Oct2 levels[3]. However, the exact pathways for these specific effects remain elusive. Our findings suggest that exposure to inward SMFs upregulates the p38 MAPK pathway and induces G1/S phase arrest, resulting in tubular epithelial injury and subsequent fibrosis. Phosphorylated p38 MAPK, an essential pro-inflammatory element, is recognized for upregulating cytokines such as interleukin-6 (IL-6) and tumor necrosis factor-α (TNF-α)[29]. ROS are critical second messengers in the p38 MAPK pathway that modulates MAPK activation via positive feedback. This process involving ROS generation and p38 activation, further enhances p53-mediated apoptosis[30].

AKI can lead to DNA damage caused by oxidative stress from ROS[31]. Under oxidative stress, 8-oxo-G is generated in DNA and subsequently released during repair by the DNA glycosylase OGG1[32]. The expression of the OGG1 gene is likely upregulated in response to oxidative stress, which aligns with our observations. Activation of p38 by cellular stress commonly leads to cell cycle arrest or apoptosis[33]. Several reports have shown that p38 activation results in G1 arrest[34,35]. AKI-induced DNA damage promotes the production of p21, which halts the cell cycle from G1 to S phase by binding to CDK4 and inhibiting the Cyclin D1/CDK4 complex. This action not only arrests cell cycle progression but also triggers the p53-dependent apoptosis pathway[36,37].

Suppressing p38 MAPK activity has been found to moderately decelerate disease progression. Li et al. and An et al. showed an elevation in pp38 MAPK after disease induction in both in-vitro and in-vivo models, alongside a dose-dependent reduction in fibrosis markers with the addition of a p38 MAPK inhibitor[38–40]. Lee et al. revealed a significant increase in phosphorylated p38 MAPK activity in a UUO mouse model and showed that inhibiting p38 MAPK led to a decrease in the mRNA expression of fibrosis markers[10]. Based on these findings, we examined the protective effects of p38 MAPK inhibition in inward SMF-induced tubular damage. Blockade of p38 MAPK reduced cell cycle arrest and apoptosis, as well as decreased the expression of fibrosis markers.

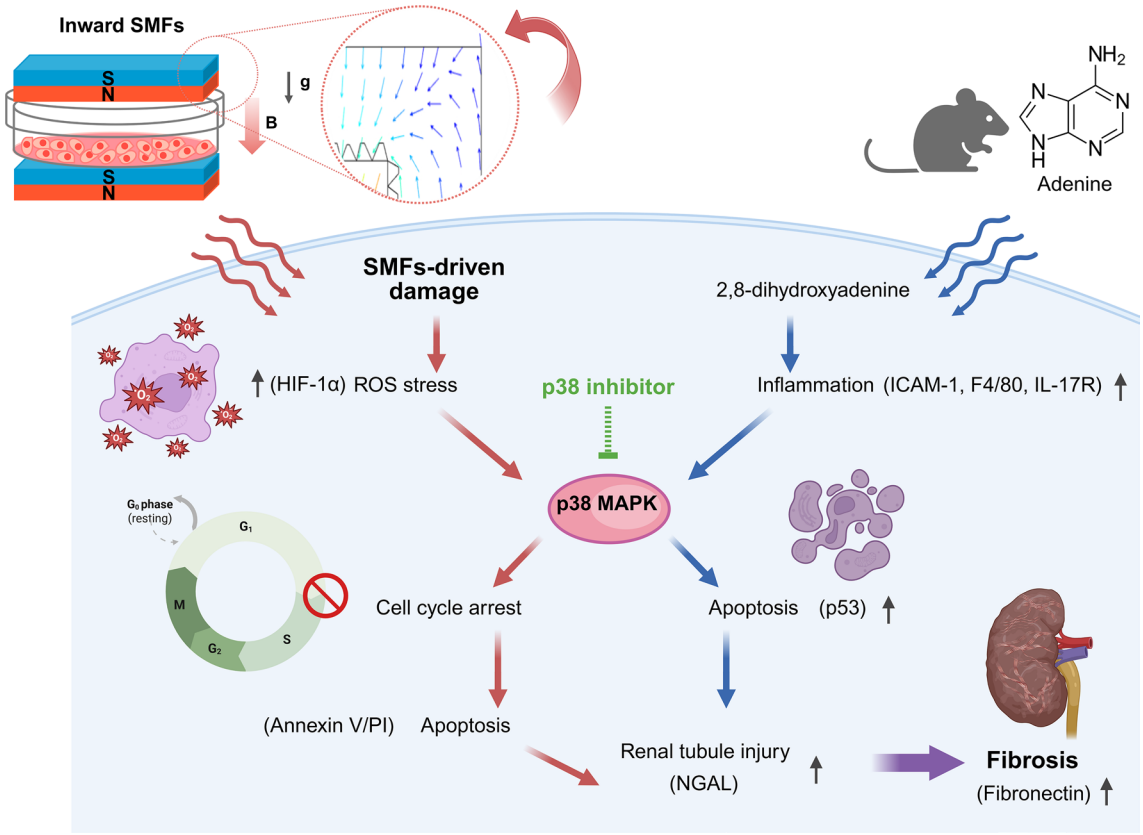

Fig. 4. Schematic illustration of cell cycle alterations and MAPK pathway involvement in the transition from SMF-induced acute renal tubular injury to fibrosis. SMF-driven damage exacerbated ROS-induced apoptosis in renal tubule injury, ultimately leading to fibrosis.

This supports prior findings that the aggravation in kidney injury and fibrosis is, particularly mediated by the p38 MAPK pathway.

To confirm the role of the p38 MAPK pathway in acute renal tubular injury and fibrosis, we established the in-vivo AITN model. When metabolized to 2,8-dihydroxyadenine (DHA), adenine accumulates crystal deposits in the renal tubules, contributing to CKD[41]. Orally ingested adenine tends to accumulate more extensively than other purines and has been frequently used to induce gradual kidney damage[41]. Adenine is rapidly metabolized to DHA, leading to crystal formation in the proximal tubule, which closely resembles human CKD[42]. Adenine treatment resulted in increased levels of kidney function biomarkers and profibrogenic markers[43,44]. This condition is characterized by diminished renal function, tubular dilation, infiltration of macrophages, and fibrosis[45,46]. In line with these observations, we validated these findings with histological analysis, indicating a significant increase in expression of ICAM-1, F4/80, NGAL, interleukin-17 receptor (IL-17R), and p53 in the in-vivo AITN model. Notably, p38 MAPK inhibition attenuated pathological changes by reducing inflammatory cell infiltration and fibrosis-related marker expression. Western blot analysis further confirmed that p38 MAPK inhibition lowered the pp38/p38 ratio and downregulated the expression of fibronectin, NGAL, and p53. Additionally, phosphorylated ERK and JNK were also reduced, indicating that p38 inhibition exerts more extensive suppressive effects across the MAPK signaling cascade. Furthermore, we assessed the antifibrotic effects of p38 MAPK inhibition in the in-vitro AITN model under inward SMF exposure.

This study opens up several avenues for further investigation. First, the effects of dynamic magnetic fields on tubular epithelial cells remain unexplored and will be a focus of future research. Second, the impact of inward SMFs and the inhibition of p38 MAPK in the AITN mouse model has not yet been fully confirmed, providing another important direction for subsequent studies. Acknowledging the scope for further exploration, we intend to address these aspects in upcoming research efforts.

In summary, our study reveals that acute tubular cell injury under inward SMFs, associated with inflammation, oxidative stress, and apoptosis, progresses to chronic fibrosis through maladaptive repair mechanisms, including G1/S cell cycle arrest and activation of the MAPK pathway (Fig. 4). Additionally, inhibiting p38 MAPK effectively mitigated AITN- and inward SMF-induced kidney injury, preventing the progression to fibrosis, which is a common final pathway in the development of CKD. These findings indicate that targeting the p38 MAPK pathway may offer a promising therapeutic approach to control the progression from inward SMF-associated AKI-to-CKD.

Methods

Establishment and measurement of strength and directions of SMFs

Human proximal tubular cells were placed between two ferrite magnets (length × width × height: 60 × 30 × 10 mm) positioned in different orientations: vertically upward SMFs opposing gravity vs. vertically downward SMFs aligning with gravity. Cells were exposed to SMFs for 3–7 days in a cell incubator (Eppendorf, Hamburg, Germany) at 37 °C and 5% CO_2. We used a digital Gauss meter (cat. MG-3002, Lutron Electronics, Coopersburg, PA, USA) to measure the magnetic field strength (mT; Tesla) within the culture plate, considering various configurations[1].

SMF simulation

A magnetic field simulation was conducted utilizing the ANSYS 2023 R2 magnetostatic (Ansys Inc., USA) program. The geometry was constructed with two magnets ($60 \times 30 \times 10$ mm^3) spaced 15 mm apart on the z-axis. In this simulation, the coercive force was set to 3.5×10^5 A/m and the residual induction was set to 450 mT. Within the Magnetostatic program, the N and S poles of the magnet were set for the upward and downward SMF conditions. As both the Petri dish and the cells located between the magnets were non-magnetic objects that did not affect the SMF, the space between the magnets was set to air with an isotropic relative permeability of 1. The mesh of the magnets was composed of 972 hexahedron meshes, whereas the exterior region, excluding the magnets (dimensions: $100 \times 70 \times 65$ mm^3), constituted 81,895 tetrahedron meshes.

Cell culture

hTECs and human kidney-2 (HK-2) cells (CRL-2190, American Type Culture Collection, Manassas, VA, USA) were used in this study for in-vitro experiments. HK-2 cells were cultured in DMEM/F12 supplemented with 10% fetal bovine serum (cat. S1480, BioWest, Nuaillé, France) and 1% penicillin/streptomycin (cat. 15,140-122, Gibco, Billings, MT, USA). Primary hTECs were harvested and cultured following the procedures outlined in our previous studies[10,35,47,48]. According to the protocol approved by the Institutional Review Board of Seoul National University Hospital (IRB No. 2110-026-1260), hTECs were isolated from normal tissue specimens obtained from resected kidneys of patients with renal cell carcinoma. Informed consent was obtained from all patients. All procedures were conducted in accordance with the ethical standards of the institutional and national research committee, as well as the 1964 Declaration of Helsinki and its subsequent amendments or comparable ethical guidelines. Following the dissection of the cortex, the tissues were minced and digested in Hank's balanced salt solution containing collagenase (1.5 mg/mL; cat. SCR103, Sigma-Aldrich, St. Louis, MO, USA) at 37 °C for 1 h. A p38 MAPK inhibitor (iP38) (0.1 μM and 1 μM; SB203580, cat. S8307, Sigma-Aldrich) was used to investigate the AKI-to-CKD mechanism under SMFs. In addition, hTECs were treated with adenine (2 mM; cat. A8626, Sigma-Aldrich) within inward SMFs for 3 days to assess the impact of SMFs on the AITN model.

Western blot analysis

Proteins were extracted from the hTECs and kidney tissue using RIPA buffer (cat. RC2002-050-00, Biosesang, Yongin, South Korea, 150 mM NaCl; 100 mM Na_3VO_4; 50 mM Tris; HCL, pH 7.3; 0.1 mM EDTA 1% (vol/vol) sodium deoxycholate; 1% (vol/vol) Triton X-100; and 0.2% NaF) with protease inhibitor (GeneDEPOT, Katy, TX, USA). BCA assay was used to standardize the protein lysates to equal concentration using Pierce BCA Protein Assay Kits (cat. 23,227, Thermo Fisher Scientific, Waltham, MA, USA). The protein samples were separated in glycine-SDS buffer and then transferred onto polyvinylidene difluoride membranes (Millipore, Bedford, MA, USA). The membranes were blocked with a solution containing 5% skim milk and 2% BSA for 1 h at 25 °C and incubated with primary antibodies (Table S1). Next, the membranes were incubated with anti-mouse IgG (cat. 7076S, Cell Signaling Technology, Danvers, MA, USA) or anti-rabbit IgG (cat. 7074S, Cell Signaling Technology) for 1 h at 25 °C. Target proteins were identified with the Fusion FX Chemi Image system (Vilber, Marne-la-Vallée, France) and subsequent analysis was performed using ImageJ (v. 1.52, Wayne Rasband, National Institutes of Health).

Immunofluorescence assay

hTECs were cultured on 4-well culture slides (Nunc Lab-Tek II Chamber Slide System, cat. 154,526, Thermo Fisher Scientific) with total media for 1 day. After replacing with new total media, cells were exposed to SMFs for 3 days. Cells on culture slides were washed with phosphate-buffered saline (PBS), fixed with 4% paraformaldehyde for 30 min, and permeabilized with 0.01% Triton X. Blocking agent containing 5% normal goat serum and 2% bovine serum albumin was used and incubated for 1 h at 25 °C. The slides were stained with antibodies overnight at 4 °C (Table S1), followed by incubation with Alexa 488-conjugated goat anti-mouse (cat. A-11001, Thermo Fisher Scientific) and Alexa 555-conjugated goat anti-rabbit (cat. A-21428, Thermo Fisher Scientific) secondary antibodies for 1 h at 25 °C. 4′,6-Diamidino-2-phenylindole (cat. D1306, Invitrogen, Waltham, MA, USA) was used for nuclear staining.

RNA isolation and real-time qPCR analysis

Total RNA from hTECs was extracted using the TRIzol reagent (Thermo Fischer Scientific) according to the manufacturer's instructions. cDNA was synthesized from the total RNA of hTECs and amplified via PCR with a C1000 thermal cycler (Bio-Rad, Hercules, CA, USA). Afterward, qPCR was performed on a 7500 Real-Time PCR System (Applied Biosystems, Waltham, MA, USA) with the following thermal cycling conditions: 50 °C for 2 min, 95 °C for 10 min, 40 cycles of 95 °C for 15 s and 60 °C for 1 min, 95 °C for 15 s, 60 °C for 1 min, 95 °C for 30 s, and 60 °C for 15 s. Relative gene expression levels were quantified using the comparative CT (ΔΔCT)

method, with GAPDH serving as the normalization control. The forward and reverse primer sequences used in this study are listed in Table S2.

Cell cycle analysis

Cells were fixed with ice-cold 70% ethanol for at least 1 h at – 20 °C and then washed with cell staining buffer (cat. 420,201, BioLegend, San Diego, CA, USA). Cells were stained with APC-conjugated Ki-67 antibody (cat. 350,514, BioLegend, 5 µL /1 × 10^6 cells in 100 µL) for 30 min at 25 °C in the dark. To ensure selective staining of DNA, cells were treated with 100 µg/mL ribonuclease (cat. GE6228, Glentham Life Sciences, Corsham, UK). PI solution (cat. 421,301, BioLegend) was used to assess DNA content in cell cycle analysis using flow cytometry. The cell cycle was evaluated through flow cytometry using a BD FACSLyric (BD Biosciences, Franklin Lakes, NJ, USA) and analyzed with FlowJo software (v10.8.1., BD Biosciences).

ROS assay

To evaluate intracellular oxidative stress, ROS levels were measured with the OxiSelect™ Intracellular ROS Assay Kit (cat. STA-342, Cell Biolabs, San Diego, CA, USA). hTECs cultured under inward SMFs and treated with iP38 (0.1 µM, 1 µM) for 3 days were incubated with 2′,7′-dichlorodihydrofluorescein diacetate (DCFH-DA) for 1 h at 37 °C. Fluorescence intensity was measured using a multi-detection analyzer (Synergy Neo2, Agilent Technologies, Santa Clara, CA, USA).

Cell apoptosis assay

To assess cell apoptosis and necrosis, the Annexin V/propidium iodide fluorescein isothiocyanate (FITC) apoptosis kit (cat. 556,547, BD Biosciences) was used for flow cytometry, following the manufacturer's instructions. After SMF exposure, harvested cells were washed with PBS, resuspended in 1X binding buffer (100 µL), and stained with FITC-conjugated Annexin V (3.5 µL) and PI (3.5 µL, 50 mg/mL). Subsequently, the cells were incubated for 15 min at 25 °C in the dark. Flow cytometry data were acquired using the BD FACSCanto (BD Biosciences) and analyzed with FlowJo software (v10.8.1., BD Biosciences).

AITN model

C57BL/6 mice (male, 8 weeks old, n = 5 per group) were obtained from KOATECH (South Korea) and adenine (2 mg/mouse, cat. A8626, Sigma-Aldrich) was orally administered daily for 2 weeks. To evaluate the effects of p38 inhibition, mice were divided into single-injection (Adenine + iP38_S) and double-injection groups (Adenine + iP38_D). In the single-injection group, mice were administered an intraperitoneal injection of p38 inhibitor (iP38; 10mg/kg, SB203580, cat. S8307, Sigma-Aldrich) 1 h prior to the first administration of adenine on day 0. In the double-injection group, the same dose of iP38 was administered on both day 0 and 5. After 2 weeks, the mice were anesthetized by intraperitoneal injection of Zoletil™ (30 mg/kg; Virbac, Carros, France) and xylazine (Rompun; 10 mg/kg; Bayer, Leverkusen, Germany), followed by sacrifice via abdominal aortic puncture for blood collection[49]. BUN (mg/dL) and creatinine (mg/dL) concentrations were measured to assess renal function using an autoanalyzer (HITACHI7180, Hitachi Chemical Industries, Tokyo, Japan). All animal studies were performed under the guidance of the Institutional Animal Care and Use Committee (IACUC: 24-0057-S1A1) of Seoul National University Hospital and conducted in accordance with the National Research Council's Guidelines for the Care and Use of Laboratory Animals. All methods for animal experiments are reported according to the ARRIVE guidelines (https://arriveguidelines.org).

Immunohistochemistry

Kidney tissues were fixed in 10% buffered formalin and embedded in paraffin. Then, 4-µm- thick sections were cut from the paraffin blocks for dehydration and rehydration, involving a series of xylene treatments followed by decreasing concentrations of ethanol and water. For antigen retrieval, the kidney sections were microwaved in sodium citrate buffer. To block endogenous peroxidase activity, a 3% hydrogen peroxide solution diluted in methyl alcohol was applied. The sections were incubated overnight at 4 °C with primary antibodies (Table S1). Subsequently, Dako Envision + System-HRP-labeled polymer anti-mouse (cat. K4001, Agilent DAKO, Santa Clara, CA, USA) and anti-rabbit (cat. K4003, Agilent DAKO) were applied and incubated for 1 h at 25°C. Periodic acid-Schiff staining was performed to evaluate tubular injury scores based on the percentage of the affected area, with cell nuclei counterstained using Mayer's hematoxylin (Sigma-Aldrich). The degree of tubular injury was assessed as previously described. The injury scores were categorized as follows: 0 for no damage, 1 for 1–10% injured area, 2 for 11–25%, 3 for 26–75%, and 4 for more than 75% injured area[45,50–52]. A Leica inverted microscope (Leica Camera, Wetzlar, Germany) and LAS-4000 software (Leica Camera) were used to analyze and quantify the affected area.

Statistical analysis

The data are presented as means with standard error of the mean. Each experiment was repeated at least three times independently. Statistical analysis was conducted using an unpaired two-tailed Student's t test in GraphPad Prism 10.0 (GraphPad Software Inc., San Diego, CA, USA). A *P*-value of less than 0.05 was considered significant ($^*P < 0.05$, $^{**}P < 0.01$, $^{***}P < 0.001$).

Data availability

The datasets generated during and/or analysed during the current study are available from the corresponding author on reasonable request.

Received: 7 April 2025; Accepted: 25 June 2025

Published online: 10 July 2025

References

1. Zhang, L. et al. 1 T moderate intensity static magnetic field affects Akt/mTOR pathway and increases the antitumor efficacy of mTOR inhibitors in CNE-2Z cells. *Sci. Bull.* **60**, 2120–2128 (2015).
2. Milovanovich, I. D. et al. Homogeneous static magnetic field of different orientation induces biological changes in subacutely exposed mice. *Environ. Sci. Pollut. Res. Int.* **23**, 1584–1597 (2016).
3. Yu, X. et al. Static magnetic fields protect against cisplatin-induced kidney toxicity. *Antioxidants (Basel)* **12**, 73 (2022).
4. Hsu, R. K., McCulloch, C. E., Dudley, R. A., Lo, L. J. & Hsu, C. Y. Temporal changes in incidence of dialysis-requiring AKI. *J. Am. Soc. Nephrol.* **24**, 37–42 (2013).
5. Guo, R. et al. The road from AKI to CKD: molecular mechanisms and therapeutic targets of ferroptosis. *Cell Death Dis.* **14**, 426 (2023).
6. Coca, S. G., Singanamala, S. & Parikh, C. R. Chronic kidney disease after acute kidney injury: a systematic review and meta-analysis. *Kidney Int.* **81**, 442–448 (2012).
7. Sugiyama, N., Kohno, M. & Yokoyama, T. Inhibition of the p38 MAPK pathway ameliorates renal fibrosis in an NPHP2 mouse model. *Nephrol. Dial. Transplant.* **27**, 1351–1358 (2012).
8. Tao, Y. et al. Nr4a1 promotes renal interstitial fibrosis by regulating the p38 MAPK phosphorylation. *Mol. Med.* **29**, 63 (2023).
9. Wang, D. et al. Inhibition of p38 MAPK attenuates renal atrophy and fibrosis in a murine renal artery stenosis model. *Am. J. Physiol. Renal Physiol.* **304**, F938–F947 (2013).
10. Lee, J. et al. p38 MAPK activity is associated with the histological degree of interstitial fibrosis in IgA nephropathy patients. *PLoS ONE* **14**, e0213981 (2019).
11. Falke, L. L., Gholizadeh, S., Goldschmeding, R., Kok, R. J. & Nguyen, T. Q. Diverse origins of the myofibroblast—implications for kidney fibrosis. *Nat. Rev. Nephrol.* **11**, 233–244 (2015).
12. Reiss, A. B. et al. Fibrosis in chronic kidney disease: pathophysiology and therapeutic targets. *J. Clin. Med.* **13**, 1881 (2024).
13. Nakanishi, T. & Kuragano, T. Growing concerns about using hypoxia-inducible factor prolyl hydroxylase inhibitors for the treatment of renal anemia. *Clin. Kidney J.* **17**, sfae051 (2024).
14. Liu, K. H. et al. Hypoxia stimulates the epithelial-to-mesenchymal transition in lung cancer cells through accumulation of nuclear β-catenin. *Anticancer Res.* **38**, 6299–6308 (2018).
15. Hu, J. et al. Hypoxia inducible factor-1α mediates the profibrotic effect of albumin in renal tubular cells. *Sci. Rep.* **7**, 15878 (2017).
16. Kimura, K. et al. Stable expression of HIF-1alpha in tubular epithelial cells promotes interstitial fibrosis. *Am. J. Physiol. Renal Physiol.* **295**, F1023–F1029 (2008).
17. Wang, Z. et al. Silencing of hypoxia-inducible factor-1α gene attenuates chronic ischemic renal injury in two-kidney, one-clip rats. *Am. J. Physiol. Renal Physiol.* **306**, F1236–F1242 (2014).
18. Yu, L. et al. HIF-1α alleviates high-glucose-induced renal tubular cell injury by promoting Parkin/PINK1-mediated mitophagy. *Front. Med. (Lausanne)* **8**, 803874 (2021).
19. Shu, S. et al. Hypoxia and hypoxia-inducible factors in kidney injury and repair. *Cells* **8**, 207 (2019).
20. Conde, E. et al. HIF-1α induction during reperfusion avoids maladaptive repair after renal ischemia/reperfusion involving miR127-3p. *Sci. Rep.* **7**, 41099 (2017).
21. Wang, J. et al. Inhibition of viability, proliferation, cytokines secretion, surface antigen expression, and adipogenic and osteogenic differentiation of adipose-derived stem cells by seven-day exposure to 0.5 T static magnetic fields. *Stem Cells Int.* **2016**, 7168175 (2016).
22. Luo, Y. et al. Moderate intensity static magnetic fields affect mitotic spindles and increase the antitumor efficacy of 5-FU and Taxol. *Bioelectrochemistry* **109**, 31–40 (2016).
23. Sullivan, K., Balin, A. K. & Allen, R. G. Effects of static magnetic fields on the growth of various types of human cells. *Bioelectromagnetics* **32**, 140–147 (2011).
24. Tian, X. et al. Magnetic field direction differentially impacts the growth of different cell types. *Electromagn. Biol. Med.* **37**, 114–125 (2018).
25. Li, J. et al. ERK and p38 MAPK inhibition controls NF-E2 degradation and profibrotic signaling in renal proximal tubule cells. *Life Sci.* **287**, 120092 (2021).
26. Yu, Q. et al. Mitogen activated protein kinase phosphatase 5 alleviates liver ischemia-reperfusion injury by inhibiting TAK1/JNK/p38 pathway. *Sci. Rep.* **13**(1), 11110 (2023).
27. Stambe, C. et al. Activation and cellular localization of the p38 and JNK MAPK pathways in rat crescentic glomerulonephritis. *Kidney Int.* **64**, 6 (2003).
28. Yang, X. et al. An upward 9.4 T static magnetic field inhibits DNA synthesis and increases ROS-P53 to suppress lung cancer growth. *Transl. Oncol.* **14**, 101103 (2021).
29. Ganguly, P., Macleod, T., Wong, C., Harland, M. & McGonagle, D. Revisiting P38 mitogen-activated protein kinases (MAPK) in inflammatory arthritis: a narrative of the emergence of MAPK-activated protein kinase inhibitors (MK2i). *Pharmaceuticals (Basel)* **16**, 1286 (2023).
30. Yue, J. & López, J. M. Understanding MAPK signaling pathways in apoptosis. *Int. J. Mol. Sci.* **21**, 2346 (2020).
31. van der Slikke, E. C. et al. Sepsis is associated with mitochondrial DNA damage and a reduced mitochondrial mass in the kidney of patients with sepsis-AKI. *Crit. Care* **25**, 36 (2021).
32. Chernikov, A. V., Gudkov, S. V., Usacheva, A. M. & Bruskov, V. I. Exogenous 8-oxo-7,8-dihydro-2′-deoxyguanosine: biomedical properties, mechanisms of action, and therapeutic potential. *Biochemistry (Mosc)* **82**, 1686–1701 (2017).
33. Kim, J. Y. et al. Involvement of p38 mitogen-activated protein kinase in the cell growth inhibition by sodium arsenite. *J. Cell. Physiol.* **190**, 29–37 (2002).
34. Whitaker, R. H. & Cook, J. G. Stress relief techniques: p38 MAPK determines the balance of cell cycle and apoptosis pathways. *Biomolecules* **11**, 1444 (2021).
35. Faust, D. et al. Differential p38-dependent signalling in response to cellular stress and mitogenic stimulation in fibroblasts. *Cell Commun. Signal.* **10**, 6 (2012).
36. Zamir-Nasta, T., Razi, M., Shapour, H. & Malekinejad, H. Roles of p21, p53, cyclin D1, CDK-4, estrogen receptor α in aflatoxin b1-induced cytotoxicity in testicular tissue of mice. *Environ. Toxicol.* **33**, 385–395 (2018).
37. Amin, M., Razi, M., Sarrafzadeh-Rezaei, F., Shalizar Jalali, A. & Najafi, G. Berberine inhibits experimental varicocele-induced cell cycle arrest via regulating cyclin D1, cdk4 and p21 proteins expression in rat testicles. *Andrologia* **50**, e12984 (2018).
38. An, J. N. et al. Periostin induces kidney fibrosis after acute kidney injury via the p38 MAPK pathway. *Am. J. Physiol. Renal Physiol.* **316**, F426–F437 (2019).
39. Li, J. et al. Inhibition of p38 mitogen-activated protein kinase and transforming growth factor-beta1/Smad signaling pathways modulates the development of fibrosis in adriamycin-induced nephropathy. *Am. J. Pathol.* **169**, 1527–1540 (2006).
40. Stambe, C. et al. Blockade of p38alpha MAPK ameliorates acute inflammatory renal injury in rat anti-GBM glomerulonephritis. *J. Am. Soc. Nephrol.* **14**, 338–351 (2003).
41. Choi, J. et al. In vivo longitudinal 920 nm two-photon intravital kidney imaging of a dynamic 2,8-dha crystal formation and tubular deterioration in the adenine-induced chronic kidney disease mouse model. *Biomed. Opt. Express* **14**, 1647–1658 (2023).

42. Khan, M. A. et al. Adenine overload induces ferroptosis in human primary proximal tubular epithelial cells. *Cell Death Dis.* **13**, 104 (2022).
43. Awad, A. M., Saleh, M. A., Abu-Elsaad, N. M. & Ibrahim, T. M. Erlotinib can halt adenine induced nephrotoxicity in mice through modulating ERK1/2, STAT3, p53 and apoptotic pathways. *Sci. Rep.* **10**, 11524 (2020).
44. Jia, T. et al. A novel model of adenine-induced tubulointerstitial nephropathy in mice. *BMC Nephrol.* **14**, 116 (2013).
45. Yoo, K. D. et al. Role of the CCL20/CCR6 axis in tubular epithelial cell injury: kidney-specific translational insights from acute kidney injury to chronic kidney disease. *FASEB J.* **38**, e23407 (2024).
46. Park, J. Y. et al. Blockade of STAT3 signaling alleviates the progression of acute kidney injury to chronic kidney disease through antiapoptosis. *Am. J. Physiol. Renal Physiol.* **322**, F553–F572 (2022) (Published correction appears in Am. J. Physiol. Renal Physiol. 323, F700 (2022)).
47. Lee, J. et al. Antibiotic-induced intestinal microbiota depletion can attenuate the acute kidney injury to chronic kidney disease transition via NADPH oxidase 2 and trimethylamine-N-oxide inhibition. *Kidney Int.* **105**, 1239–1253 (2024).
48. Park, S. et al. Elevated bilirubin levels are associated with a better renal prognosis and ameliorate kidney fibrosis. *PLoS ONE* **12**, e0172434 (2017).
49. An, J. N. et al. cMet agonistic antibody attenuates apoptosis in ischaemia-reperfusion-induced kidney injury. *J. Cell. Mol. Med.* **24**, 5640–5651 (2020).
50. Jang, H. R. et al. Early exposure to germs modifies kidney damage and inflammation after experimental ischemia-reperfusion injury. *Am. J. Physiol. Renal Physiol.* **297**, F1457–F1465 (2009).
51. Yoo, K. D. et al. Chemokine receptor 5 blockade modulates macrophage trafficking in renal ischaemic-reperfusion injury. *J. Cell. Mol. Med.* **24**, 5515–5527 (2020).
52. Lobel, L. et al. Diet posttranslationally modifies the mouse gut microbial proteome to modulate renal function. *Science* **369**, 6510 (2020).

Acknowledgements

Illustrations in Fig. 3a, Fig. 4, and Fig. S1a were created with BioRender.com.

Author contributions

SML, SRL, SHL, EJB, KDY, JWL, YSK, R-hC, and SHY designed the experiments. SML, SRL, KHK, SJP, and KHK performed the research. All authors analyzed the data. SML and SRL wrote the paper. R-hC and SHY designed and supervised the project. All authors reviewed the manuscript.

Funding

This research was funded by the National Research Foundation of Korea grant (NRF-2023R1A2C2006651) and Seoul National University Hospital (No. 3020240100).

Declarations

Competing interests

The authors declare no competing interests.

Ethical approval

All animal experiments were conducted in accordance with the guidelines of the Institutional Animal Care and Use Committee of Seoul National University Hospital (IACUC approval number: 24-0057-S1A1). Human kidney biopsy samples were collected with approval from the Institutional Review Board of Seoul National University Hospital (IRB approval number: 2110-026-1260), and informed consent was obtained from all patients.

Additional information

Supplementary Information The online version contains supplementary material available at https://doi.org/10.1038/s41598-025-09077-w.

Correspondence and requests for materials should be addressed to R.-h.C. or S.H.Y.